

# Nanoscale

Accepted Manuscript



This is an *Accepted Manuscript*, which has been through the Royal Society of Chemistry peer review process and has been accepted for publication.

*Accepted Manuscripts* are published online shortly after acceptance, before technical editing, formatting and proof reading. Using this free service, authors can make their results available to the community, in citable form, before we publish the edited article. We will replace this *Accepted Manuscript* with the edited and formatted *Advance Article* as soon as it is available.

You can find more information about *Accepted Manuscripts* in the [Information for Authors](#).

Please note that technical editing may introduce minor changes to the text and/or graphics, which may alter content. The journal's standard [Terms & Conditions](#) and the [Ethical guidelines](#) still apply. In no event shall the Royal Society of Chemistry be held responsible for any errors or omissions in this *Accepted Manuscript* or any consequences arising from the use of any information it contains.



## Evidence does not support absorption of intact solid lipid nanoparticles via oral delivery

Received 00th January 20xx,  
Accepted 00th January 20xx

Xiongwei Hu,<sup>a</sup> Wufa Fan,<sup>a</sup> Zhou Yu,<sup>a</sup> Yi Lu,<sup>a</sup> Jianping Qi,<sup>a</sup> Jian Zhang,<sup>a</sup> Xiaochun Dong,<sup>a</sup> Weili Zhao,<sup>a,b†</sup> and Wei Wu<sup>a†</sup>

DOI: 10.1039/x0xx00000x

www.rsc.org/

Whether and to what extent solid lipid nanoparticles (SLNs) can be absorbed integrally via oral delivery should be clarified because it is the basis for elucidation of absorption mechanisms. To address this topic, *in vivo* fate of SLNs as well as their interaction with biomembranes is investigated using water-quenching fluorescent probes that can signal structural variations of lipid-based nanocarriers. Live imaging indicates prolonged retention of SLNs in stomach, whereas in intestine SLNs can be digested quickly. No translocation of intact SLNs to other organs or tissues can be observed. *In situ* perfusion study shows bioadhesion of both SLNs and simulated mixed micelles (SMMs) to intestinal mucus, but no evidence of penetration of integral nanocarriers. Both SLNs and SMMs exhibit significant cellular uptake, but fail to penetrate cell monolayers. Confocal laser scanning microscopy reveals that nanocarriers mainly enrich on the surface of the monolayers, and no evidence of penetration of intact vehicles can be obtained. The mucous layer presents as a barrier to the penetration of both SLNs and SMMs. Both bile salt-decoration and SMMs formulation help to strengthen the interaction with biomembranes. It is concluded that evidence does not support absorption of intact SLNs via oral delivery.

### Introduction

Lipid nanoparticles refer to a class of nanocarriers that are mainly made up of a certain kind of lipid or lipid mixtures. Common lipid nanoparticles are roughly classified into solid lipid nanoparticles (SLNs), nanostructured lipid carriers (NLCs), whose compositions are comprised of a mixture of solid and liquid lipids, and nanoemulsions or "microemulsions", which are principally made of liquid lipids with surfactants as stabilizers.<sup>1-4</sup> Due to relatively small size and resemblance in compositions to biomembranes, lipid nanoparticles show great potential as drug carriers with high loading capacity, improved dissolution and enhanced permeation across biomembranes.<sup>5-8</sup> Partly because of their ability to mimic the digestive process of food-based lipids in the gastrointestinal (GI) tract, lipid nanoparticles have drawn

much attention in enhancing oral bioavailability of poorly water-soluble drugs.<sup>9-15</sup>

Despite of the prosperity in formulation development, the research on *in vivo* performance and mechanisms of action of lipid nanoparticles lags far behind. It is believed that exploring the *in vivo* fate of lipid nanoparticles facilitates translation into clinical use. However, this task has been proved to be extraordinarily difficult owing to the complexity of body physiology and extremely small size that makes recovery or detection of lipid nanoparticles very difficult. Blind as we are, we just manage to fumble a toe of a giant elephant. As for oral delivery, the situation is even worse and more challengeable because the presence of food, intrinsic surfactants and enzymes interferes significantly with identification of nanoparticles.

Based on understanding of the digestive mechanism of food-originated lipids,<sup>16,17</sup> lipolysis was proposed as the principle mechanism governing the oral fate of lipid nanoparticles.<sup>18,19</sup> It is known that ingested oil or fat is generally churned in the stomach to form fine droplets, which are further transported to the small intestine to be digested by lipases together with co-lipases. Lipid nanoparticles seemingly can be transported directly into small intestine and be processed there through lipolysis.<sup>17</sup> Lipid lysate generated this way, mainly monoglycerides and

<sup>a</sup> School of Pharmacy, Fudan University, Key Laboratory of Smart Drug Delivery of MOE and PLA, Shanghai 201203, China

<sup>b</sup> Key Laboratory for Special Functional Materials of the Ministry of Education, Henan University, Kaifeng 475001, China

† Corresponding author. E-mail: wuwei@shmu.edu.cn; zhaowei@fudan.edu.cn  
Electronic Supplementary Information (ESI) available. See  
DOI: 10.1039/x0xx00000x

fatty acids, is able to form mixed micelles with the help of physiologically secreted phospholipids and bile salt (BS) derivatives.<sup>16,17</sup> In the meantime, the payload of lipid nanoparticles can be transferred into mixed micelles and absorbed through either passive diffusion or lipid exchange mechanisms.<sup>17</sup> Although the lipolysis-based mechanism has been well accepted to interpret the oral fate of lipid nanoparticles, there are controversies over possibility of surviving lipolysis and subsequent absorption of intact lipid nanoparticles by enteric epithelia.<sup>20-22</sup> The intact-absorption assumption serves as the basis for several reports on enhanced oral bioavailability of various drugs by lipid nanoparticles.<sup>12,15,20,21</sup> However, this assumption is groundless because there is no persuasive evidence to date to support the mechanism of intact absorption of lipid nanoparticles via oral delivery. It is of urgency and importance to collect evidence to clarify this issue.

Several studies in Caco-2 cell lines did prove that lipid nanoparticles could facilitate permeation of their cargoes across cell monolayers.<sup>20-25</sup> However, the real situation in the GI tract may not allow direct contact of lipid nanoparticles with the enteric epithelia, and the cell line-based conclusions should be reconsidered. Workable mechanisms should be concluded from direct evidence of *in vivo* observation, together with the aid of *ex vivo*, *in situ* and cellular observations. Due to the small size of lipid nanoparticles and the versatility of various phases presented in the GI tract, it is impossible to recover lipid nanoparticles from the GI tract after oral administration. The feasible protocol to monitor lipid nanoparticles in the GI tract is through detection of functional probes that label the nanocarriers. In a pioneer work,<sup>26</sup> SLNs made of FITC-conjugated stearamine were found to be able to transit mostly to the lymphatic system by recovering FITC-based fluorescence. This finding however is challenged by logical reasoning that FITC-stearamine may dissociate from SLNs and be absorbed in its free form, which afterwards may associate with chylomicrons in enterocytes and be transported via the lymphatic route. In a recent study,<sup>27</sup> FITC signals (labelling the drug) were found penetrating deep into intestinal villi, whereas rhodamine signals (labelling the lipid) located to villi surfaces, suggesting unlikeliness of transportation of intact lipid nanoparticles into circulation. However, it is argued that the fluorescent signals cannot be taken for granted to represent either the drug or the lipids or intact nanoparticles at all because it is quite possible that the probes may have dissociated from the nanoparticles. In another study,<sup>28</sup> a near-infrared (NIR) fluorescent probe Dil-labelled SLNs were located in the epithelia and a mechanism of intact internalization was concluded. The weakness of this study lies in the fact that Dil emits fluorescence whether it is encapsulated into lipid nanoparticles or not; therefore, the conclusion of intact

uptake of SLNs has no firm basis. Signals of functional probes should be able to reflect the real-time structural alterations of the lipid nanoparticles *per se*, and should be discriminated from signals of free probes.

In our previous study, we developed a class of NIR fluorescent aza-BODIPY probes to monitor the *in vivo* fate of lipid-based nanocarriers.<sup>29</sup> The most outstanding feature of this kind of probes is their water-quenching properties upon contact with water based on the aggregation-caused quenching (ACQ) effect. Because of high lipophilicity ACQ probes can be encapsulated into the lipid matrix with little leakage. The rationale of detection is based on on  $\rightarrow$  off signal switching upon degradation of the lipid matrix and simultaneous release of the probes. Through non-invasive imaging, the *in vivo* fate of lipid nanoparticles can be monitored accurately and precisely. Whereas the previous proof-of-concept study principally focused on validation of the feasibility of ACQ probes, the current study aims to elucidate holistically the *in vivo* fate of a model lipid nanoparticles, SLNs, using live imaging equipment. Besides, *in situ* intestinal retention and transmembrane permeation across Caco-2 cell monolayers are also investigated to facilitate interpretation of the underlying absorption mechanisms. The key point of this study is that the explanations are based on signals of intact nanoparticles, excluding interference brought about by dissociated fluorescent probes.

## Experimental

### Materials

The water-quenching NIR fluorescent probes, P2 ( $\lambda_{\text{abs}}/\lambda_{\text{em}}=708/732$ ) and P4 ( $\lambda_{\text{abs}}/\lambda_{\text{em}}=651/662$ ), were synthesized according to previous procedures;<sup>30,31</sup> refer to previous publication for their physicochemical properties.<sup>29</sup> Orlistat (Hubei Yucheng Pharm Co., Ltd., China); Tween 80, stearic acid (SA), glycerol monostearate (MG), glycerin and sucrose (Sinopharm Reagent Co., Ltd., China); Food grade peanut oil (Yihai Kerry Group, China); Compound meglumine diatrizoate injection (Shanghai Xudong Haipu Pharmaceutical Co., Ltd., China); Isoflurane (Shandong Keyuan Pharmaceutical Co., Ltd., China); Precirol<sup>®</sup> ATO 5, Geleol<sup>®</sup> Pellets (Gattefossé Co., Cedex, France); Lecithin (Lipoid E100, Lipoid GmbH Company, Ludwigshafen, Germany); Sodium taurocholate (STC) (Tokyo Chemical Industry Co., Ltd., Tokyo, Japan); SIGMAFAST<sup>™</sup> fast red TR/naphthol AS-MX tablets, coumarin 6 (C6) (Sigma-Aldrich, St. Louis, USA); Lipase from porcine pancreas, Tris-maleate (Sigma-Aldrich, Shanghai, China); Simulated intestinal fluid (SIF) powder (Biorelevant.com, Croydon, United Kingdom); Glucose (Amresco, USA), sodium pyruvate (Beijing Solarbio Technology Co., Ltd., China); 4% Paraformaldehyde

(Fortunebio-tech Co., Ltd., Shanghai, China); 4',6-Diamidino-2-phenylindole (DAPI), carboxyfluorescein succinimidyl amino ester (CFSE) (Yeasen Bio-tech Co., Ltd., Shanghai, China); Rhodamine-phalloidin (Qianchen Bio-tech Co., Ltd., Shanghai, China); Alcian blue (J & K Chemical Co., Ltd., Beijing, China); OCT compound (Leika, Germany); Caco-2 cells, Raji cells (Cell Bank of Chinese Academy of Sciences, Shanghai, China); HT29-MTX (China Center for Type Culture Collection, Wuhan, China). The following reagents were purchased from Gibco (USA): Dulbecco's Modified Eagle's Medium (DMEM, containing 10% FBS, 1% non-essential amino acid, 1% penicillin-streptomycin solution), Roswell Park Memorial Institute-1640 (RPMI 1640, containing 10% FBS, NaHCO<sub>3</sub> 1.5 g/L, glucose 2.5 g/L and sodium pyruvate 0.11 g/L), fetal bovine serum (FBS), nonessential amino acids (NAA), penicillin-streptomycin solution, 0.25% trypsin-0.02% EDTA solution, Hank's balanced salt solution (HBSS), D-Hank's (HBSS without calcium and magnesium). Deionized water was prepared by a Milli-Q purification system (Millipore, USA). All solvents used for UV and fluorescence measurements were of either spectroscopic grade or HPLC grade and purchased from Acros, Aldrich or Fluka. Other reagents were of analytical grade and purchased from local distributors.

#### Preparation and characterization of fluorescent probe-labelled SLNs and simulated mixed micelles (SMMs)

SLNs were prepared by a hot homogenization method using Precirol<sup>®</sup> ATO 5 as the lipid and Tween 80 as the emulsifier following exactly the same procedures as in our previous study.<sup>29</sup> Briefly, the lipid was first heated to melt at 70°C, and the fluorescent probes, either P2 or P4 or C6 dissolved in dichloromethane (DCM), was added into the lipid phase. After thorough mixing and removal of DCM, the melted mixture was dispersed into 70°C water containing 2% (w/v) Tween 80 and homogenized first by a high-shear homogenizer (Scientz Biotechnology Co., Ltd., China), followed by a micro-jet homogenizer (Nano DeBEE, USA). The hot O/W dispersion was cooled down gradually in a water bath to obtain fluorescent SLNs. By replacing half of Tween 80 with STC as the emulsifier, BS-decorated SLNs could be obtained following the same procedures.

SMMs were prepared by a thin-film dispersion method.<sup>32,33</sup> Although the exact compositions of physiological mixed micelles have not been deciphered yet, BS and phospholipid are believed to be the two essential compositions that play important roles in the metabolism of lipids. The molar ratio of physiological BS to phospholipids is proved to be around 4:1, and has been well accepted as the basis for concoction of bio-relevant media.<sup>34-36</sup> The same ratio is adopted in this study. Briefly, dissolve 107.5 mg STC, 37.5 mg lecithin and certain amount of MG and SA in 5 mL methanol/chloroform (1:1, v/v)

mixed solvent under bath sonication; add 20 µL of P4 chloroform solution (89 µg/mL) and 100 µL of C6 chloroform solution (40 µg/mL), respectively; mix thoroughly. The organic solvent was evaporated completely by a rotatory evaporator (IKA, Germany), and subsequently a thin film of the mixture was formed in the inner wall of the flask. Upon addition of 10 mL D-Hank's, the lipid thin film was hydrated and self-assembled into P4/C6 double-labelled SMMs (P4/C6-SMMs).

Particle size of both SLNs and SMMs was measured by Zetasizer Nano<sup>®</sup> (Malvern Instruments, Malvern, UK) with a 4-mW He-Ne laser at 633 nm under ambient temperature. Entrapment efficiency (EE%) was measured using ultrafiltration cells (Amicon<sup>®</sup> Ultra-0.5, 100 kDa for SLNs and 30 kDa for SMMs, USA) following previous procedures.<sup>28</sup> Fluorescent intensity of C6 was measured directly by Cary Eclipse fluorospectrophotometer, whereas for water-quenching probes, P2 and P4, the probes were first extracted using ether, and determined by fluorospectrophotometry afterwards.

All of the fluorescent probes-labelled SLN or SMM samples were sealed and stored at 20°C and 4°C for one week. At 0, 1, 3, 5 and 7 d, the samples were characterized for particle size, polydispersity index (PDI) and fluorescent intensity, and the storage stability was evaluated.

#### Live imaging of *in vivo* fate of SLNs

Male ICR mice, weighing 20 ± 2 g, were raised in the Experimental Animal Centre of Fudan University regarding the ethical guidelines on experiments involving use of animals. Exactly 0.2 mL P2-SLNs suspension was administered by gastric gavage to the mice, and the *in vivo* fate was monitored using IVIS Spectrum Live Imaging System (PerkinElmer, USA). There are definitely four test groups i.e. the fasted (fasted for 24 h, free access to water), the fed (free access to standard food and water), the high-fat (feeding 0.2 mL peanut oil every morning and evening for 3 consecutive days before test) and the lipase-inhibition group (0.2 mL of 22 µg/mL orlistat solution dispersed in SLN dispersion, free access to standard food and water), whereas quenched P2 solution was given to either fasted or fed mice as controls. During the imaging process, animals were anesthetized by an on-line gas anesthesia system using isoflurane. In order to clearly locate the exact position of SLNs in the whole GI tract, animals were sacrificed at time intervals, and the whole GI tract was dissected and observed using IVIS imaging system at a sample thickness of 0.5 cm. The fluorescence intensity in each GI segments was quantified and compared.

Real-time positioning of nanocarriers during the whole digestion process was carried out using IVIS Spectrum Live Imaging System CT (PerkinElmer, USA). Before experiment, the ICR mice were fasted for 24 h, but

allowed free access to water. Thirty minutes before administration of SLNs, 0.1 mL compound meglumine diatrizoate injection (20%) was administered. The test samples were P2-SLNs given by gastric gavage either in low or high dose in a volume of 0.2 mL. The low dose group employed the same dose as above, whereas the high dose was 5 times that of the low dose, as concentrated by ultrafiltration. After administration, the *in vivo* fate was imaged at time intervals after anesthetization by isoflurane.

#### ***In situ* bioadhesion and *ex vivo* residence study**

Wistar rats weighing  $200 \pm 20$  g was anesthetized using phenobarbital (40 mg/kg) intraperitoneally and fixed in a supine position. A longitudinal incision of about 3 cm long was cut in the middle of the abdomen, and the small intestine was found and cannulated 15 cm to 25 cm downward from the pylorus to form a loop. The intestine loop was flushed quickly with blank K-R solution to remove the intestine content, and then with SLN or SMM suspension, diluted using K-R solution by 5 folds beforehand, following the one-direction (proximal  $\rightarrow$  distal) *in situ* perfusion procedures.<sup>37</sup> Perfusion was proceeded at 0.2 mL/min; after balancing for 30 min, about 2 mL effluent was collected every 10 min and assayed for fluorescent intensity. After perfusion, the residues in the intestinal lumen was forced out by air, and the intestinal segments was cut off immediately and observed using IVIS live imaging system.

The jejunum segment was cut into pieces of rings and fixed in 4% paraformaldehyde for 12 h, and dehydrated in 30% sucrose solution. Frozen sections of the specimen were collected after being embedded in OCT compound, stained using DAPI to mark the nucleus, and observed by Zeiss LSM 510 confocal laser scanning microscopy (CLSM) (Carl Zeiss Inc., Germany).

#### **Cell culture**

Recovered Caco-2 cells were cultured follow regular procedures in high glucose DMEM culture media at 37°C, RH 90% and 5% CO<sub>2</sub> in T-25 flasks. The culture medium was changed every other day. The cells were passaged every 3-5 d after dissociation with 0.25% trypsin/0.02% EDTA solution when cell fusion rate reached 85%. HT29-MTX cells were cultured following the same procedures, but could be in reduced culture media-changing frequency due to slow growth rate. For Raji cell culture, RPMI 1640 culture medium was used to replace DMEM and passaged every 4-6 d.

#### **Cellular uptake**

Caco-2 cells in exponential phase were seeded into black cell culture plates (for live imaging) or glass cell culture dishes (for CLSM) in a density of  $5 \times 10^4$  cells/cm<sup>2</sup> following

regular culturing procedures. Culture medium was changed every other day before intact monolayer formed and every day afterwards. After 14 d, the cell model was ready for cellular uptake study. For Caco-2/HT29-MTX cell models, both Caco-2 and HT29-MTX cells in exponential phase were slightly digested, suspended and counted; afterwards the two kinds of cells were mixed in a population ratio of 7:3,<sup>38</sup> and seeded in a density of  $1 \times 10^5$  cells/cm<sup>2</sup>. Follow the procedures below to study cellular uptake: discard the culture media; wash with D-Hank's three times; add 200  $\mu$ L SLNs or SMMs suspension in triplicates; culture for 2 h; discard the test samples; wash with D-Hank's for another three times; add 200  $\mu$ L D-Hank's into each well. The fluorescence of each well was scanned and quantified by IVIS live imaging systems or observed by CLSM.

#### **Trans-monolayer transport**

Caco-2 cells in exponential phase were seeded into the apical side of Millicell-CM insert cell culture plates (PCF film, 0.4  $\mu$ m) in a density of  $1 \times 10^5$  cells/cm<sup>2</sup> under regular culturing conditions. Culture medium was changed every other day for the first week, and everyday afterwards for a total of 21 d. Trans-epithelial electrical resistance (TEER) was measured, and a threshold value of 300  $\Omega \cdot \text{cm}^2$  was set for transmembrane studies.

Following exactly the same procedures, Caco-2/HT29-MTX monolayers were cultured, but with a Caco-2/HT29-MTX population ratio of 7:3.<sup>38</sup> The seeding of HT29-MTX cells was validated by alcian blue staining. Briefly, follow the procedures: discard the culture media in the Caco-2/HT29-MTX monolayer model; wash with PBS once; add alcian blue 8GX solution; cultivate for 30 min at room temperature; discard the staining solution; wash with PBS once; add Fast Red TR/Naphthol AS-MX solution; cultivate for 20 min at room temperature; wash with PBS once. The monolayers were observed under inverted fluorescence microscope, and blue staining confirmed the formation of a mucus layer on the surface of the monolayers.

For establishment of the Caco-2/Raji co-culture monolayer model, Caco-2 cell monolayers with TEER over 300  $\Omega \cdot \text{cm}^2$  were further cultured for 5 d after addition of Raji cells to the basal side in a density of  $2 \times 10^6$  cells/mL.<sup>39</sup> TEER values were monitored each day until significant decrease in TEER was observed, which indicated successful infiltration of Raji cells. To validate, green-stained Raji cells were used to infiltrate the cell monolayers, and the basal side of the culture film was observed by CLSM to identify Raji cells.

To study trans-monolayer transport, 200  $\mu$ L SLNs or SMMs suspension and 900  $\mu$ L D-Hank's were added to the apical and basal side, respectively, and cultivated for 2 h.

Samples were withdrawn from the basal side at time intervals and measured directly for fluorescence intensity.

## Results and discussion

### Preparation and characterization of SLNs and SMMs

SLNs prepared under optimum conditions have a particle size of about 75 nm and a polydispersity index of less than 0.22, similar to results in our previous study.<sup>29</sup> The zeta potential is near neutral but slightly negative possibly owing to the presence of residues of fatty acids. Due to high lipophilicity, all probes are entrapped in the lipid matrix of SLNs with high entrapment efficiency (> 90%). Since the NIR probes used in this study have very high quantum yield, a very low loading is enough to meet the requirement of detection. Within the investigated range (P2/lipid:  $1 \times 10^{-5}$  –  $8 \times 10^{-5}$ ; P4/lipid:  $2 \times 10^{-6}$  –  $1.6 \times 10^{-5}$ ), there is good linearity between fluorescence intensity and probe concentration.

Fixing the ratio of STC/lecithin at 4:1, the composition of SMMs was optimized by varying the amount of MG and SA. When there is no MG and SA at all, the particle size of SMMs is about 30 nm. The zeta potential is negative due to the presence of bile salts to the surfaces of SMMs. It is evident that the particle size as well as PDI of SMMs increases along with increase of MG and SA amount (Table 1S, 2S). Of note, bile salt-decorated SMMs have smaller particle sizes than non-decorated ones because of surface tension decreasing effect induced by bile salts. In the end, a SMM formulation with similar particle size to SLNs and relatively small PDI was selected for further studies. For

comparison, SMMs without BS was optimized by replacing STC with potassium oleate. Please refer to Table 1 for fundamental properties of both SLNs and SMMs. For *in vivo* live imaging, P2 was used to label SLNs because of its longer emission wavelength. As for *in situ* and *in vivo* studies, P4 was used to label either SLNs or SMMs due to its high quantum yield. The non-water-quenching probe C6 was used as a control, whose behaviours can be interpreted to represent the payload, e.g. drug molecules.

As discussed in our previous study, in order to accurately and precisely detect the variations of the integral structure of lipid-based nanocarriers, three prerequisites should be met: 1) the ACQ effect of the probes should be highly sensitive; 2) the degradation of lipid matrices of nanocarriers should be synchronous to the quenching of fluorescence; 3) deviation to fluorescence quenching other than bioerosion of the lipid matrices such as leakage of the probes and soaking of the matrices by water should be excluded.<sup>29</sup> As for SLNs, the three prerequisites have been well justified either by experimental results or logical reasoning. However, for SMMs the feasibility of using water-quenching probes to monitor the variations in integral structure has not been validated. Since the mixed micelles possess a simple core-shell structure, which does not apply to previous discussion on lipid matrices, the second prerequisite could be easily neglected. It is understandable that upon disruption of the mixed micelles the probes would be released and quench simultaneously due to the ACQ effect. Only when the third prerequisite is met could the water-quenching probes be well applied for mixed micelles. Therefore, it is obliged to ascertain that there is no leakage of the probes from SMMs.

Table 1 Characterization of SLNs and SMMs formulations (Mean  $\pm$  SD,  $n = 3$ )

Code	Composition	Particle Size (nm)	PDI	Zeta potential (mV)	EE (%)		Loading (%)		FL intensity (a.u.)	
					P2/P4	C6	P2/P4	C6	P2/P4	C6
Control	Aqueous dispersion of probes								0.05 $\pm$ 0.04	38.7 $\pm$ 4.2
P2-SLNs	Precirol ATO 5; Tween 80 as emulsifier	75.7 $\pm$ 5.2	0.217	-3.4 $\pm$ 0.7	94.8 $\pm$ 2.4		2.00 $\times$ 10 <sup>-3</sup> $\pm$ 5.13 $\times$ 10 <sup>-5</sup>		774.5 $\pm$ 16.4	
P4/C6-SLNs	Precirol ATO 5; Tween 80 as emulsifier	73.4 $\pm$ 4.3	0.242	-2.3 $\pm$ 0.3	92.1 $\pm$ 1.9	93.4 $\pm$ 4.1	2.34 $\times$ 10 <sup>-4</sup> $\pm$ 4.85 $\times$ 10 <sup>-6</sup>	5.34 $\times$ 10 <sup>-4</sup> $\pm$ 2.35 $\times$ 10 <sup>-5</sup>	804.3 $\pm$ 35.7	712.9 $\pm$ 46.8
BS-P4/C6-SLNs	Precirol ATO 5; Tween 80 and STC as emulsifiers	87.5 $\pm$ 5.8	0.278	-6.1 $\pm$ 0.6	90.4 $\pm$ 4.5	92.6 $\pm$ 3.7	2.30 $\times$ 10 <sup>-4</sup> $\pm$ 1.15 $\times$ 10 <sup>-5</sup>	5.29 $\times$ 10 <sup>-4</sup> $\pm$ 2.13 $\times$ 10 <sup>-5</sup>	821.9 $\pm$ 45.5	725.0 $\pm$ 41.1
P4/C6-SMMs	Potassium oleate: phospholipid: MG: SA = 4:1:0.1:0.1	75.1 $\pm$ 10.2	0.220	-36.6 $\pm$ 2.0	88.6 $\pm$ 8.9	90.2 $\pm$ 4.1	1.06 $\times$ 10 <sup>-3</sup> $\pm$ 1.07 $\times$ 10 <sup>-4</sup>	2.43 $\times$ 10 <sup>-3</sup> $\pm$ 1.11 $\times$ 10 <sup>-4</sup>	712.5 $\pm$ 70.4	803.2 $\pm$ 44.3
BS-P4/C6-SMMs	STC: phospholipid: MG: SA = 4:1:0.1:0.1	50.6 $\pm$ 8.8	0.207	-23.9 $\pm$ 2.8	86.8 $\pm$ 7.7	91.4 $\pm$ 3.8	1.47 $\times$ 10 <sup>-3</sup> $\pm$ 1.31 $\times$ 10 <sup>-4</sup>	3.49 $\times$ 10 <sup>-3</sup> $\pm$ 1.46 $\times$ 10 <sup>-4</sup>	698.8 $\pm$ 56.7	823.5 $\pm$ 49.7

At 20°C the fluorescent intensity of P4 remains quite stable for all formulations up to 7 d with total fluorescent intensity over 95% (Fig. 1S). At 4°C, the fluorescent intensity of P4 for SLNs remains stable, but not for SMMs whose fluorescence intensity drops dramatically to below 85% (BS-P4/C6-SMMs) and 75% (P4/C6-SMMs), respectively, after storage for 1 d. It can be interpreted that the solubility of surfactants may decrease significantly, which thus lead to leakage of P4 and subsequent fluorescence quenching. Interestingly, the results of the C6 signals show very stable fluorescence intensity for all formulations at all temperatures, which however contradicts the P4 results of SMMs at 4°C. This alerts us that C6 signals may not be able to accurately reflect the real structural variations.

### In vivo fate of SLNs

Fig. 1A shows the live imaging pictures of *in vivo* fate of SLNs in the GI tract of mice. In agreement with our previous study,<sup>29</sup> oral administration of quenched P2 solution does not show any sign of fluorescence rekindling under both fasted and fed conditions. This eliminates concerns over the interference brought about by rekindling of quenched probes at sensitivity threshold set in this observation. For all treatment groups, fluorescent spots can be observed at the position of the abdomen, which we later locate as the GI tract, and no fluorescence can be detected at tissues other than this areas. Although variations in the position of fluorescent spots could be faintly discerned, the exact location within the GI tract can hardly be identified due to the disadvantages of 2D imaging. Despite of this, obvious difference in *in vivo* fate of SLNs could be observed for different treatment groups. Both the fasted and fed groups show fluorescence in decreasing intensity for up to 4 h, complying with previous findings in nude mice.<sup>29</sup> For the high-fat and lipase-inhibition groups, fluorescence can be detected for at least 12 h. In contrary to our assumption that beforehand administration of oil may stimulate secretion of lipases as well as a variety of physiological surfactants and expedite the degradation of subsequently administered SLNs, the high-fat group shows sustained fluorescence at very high level. The behaviours of the lipase-inhibition group are well within our expectation that delayed fluorescence quenching is observed due to suppression of GI lipase activity. Fig. 1B depicts the profiles of biodegradation kinetics through measurement of average radiant efficiency (ARE) as an indicator of total fluorescence. The fasted group follows strict first-order kinetics with regression coefficient of over 0.99, which complies well with previous results in nude mice as well as *in vitro* lipolysis test.<sup>29</sup> The fed group follows similar trend but with wide oscillation. The lipase-inhibition group showed high fluorescence levels at later stages, whereas

the high-fat group showed sustained fluorescence at very high levels for over 12 h.

In order to locate the exact transiting position of SLNs, the whole GI tract and various organs was dissected and scanned by IVIS live imaging system. It is certain that no P2 signal is detected in various organs and tissues (blood, liver, spleen, lung, kidney, brain, etc.) other than the GI tract for all treatment groups. No fluorescence is detected for quenched P2 control either under fasted or fed conditions in accord with live imaging results (Fig. 1C). However, observation with different test groups reveals unexpected findings. The most outstanding finding is that a majority of fluorescence is found in the stomach (Fig. 1C). In the fasted group, the gastric residence time is the shortest among all test groups with relatively high fluorescence intensity for just 2 h, but faint residue fluorescence for as long as 8 h, whereas the fed group shows relatively intense fluorescence for up to 8 h and faint residue fluorescence for at least 12 h. For both high-fat and lipase-inhibition groups, very strong fluorescence can be observed in the stomach for as long as over 12 h. To date there is no clear interpretation to prolonged residence of nanoparticles in the stomach. It seems that SLNs may penetrate deep into the gastric mucus and be retained there with concurrent transiting downstream upon periodical refreshing of gastric mucus. Although the transit of nanoscale particles is little affected by food, the gastric emptying rate may play a part in overall retention of SLNs. Therefore, the fasted group shows the shortest gastric residence time due to fast emptying rate. It is reported that ingestion of high doses of fat or oil may slow down the gastric emptying rate<sup>40</sup> and results in prolonged residence of SLNs in stomach. For the lipase-inhibiting group, the relatively strong residence of fluorescence may be explained by the fact that inhibition of lipases by orlistat results in presence of more fat in the GI tract which in turn inhibits gastric emptying. In sharp contrast with gastric residence, the total residence time and fluorescence intensity in small intestine are relatively low (Fig. 1D-G). Fluorescence can be found at proximal and distal ileum at 0.5 h and 1.0-2.0 h, respectively, for all test groups except the lipase-inhibition group; beyond 2 h, only faint fluorescence can be observed in the colon. The situation of the lipase-inhibiting group is more complicated as fluorescence can be observed throughout the whole intestinal tract for extended residence time of over 12 h. Based on *ex vivo* results, we can summarize that SLNs can be retained in the stomach for extended time durations and serve as a reservoir to provide continuously more SLNs to the intestinal lumen. And the gastric retention effect is strengthened in presence of food, especially with beforehand administration of oil. Since the normal gastric emptying time is about 1.5 h for mice,<sup>41</sup> the obviously

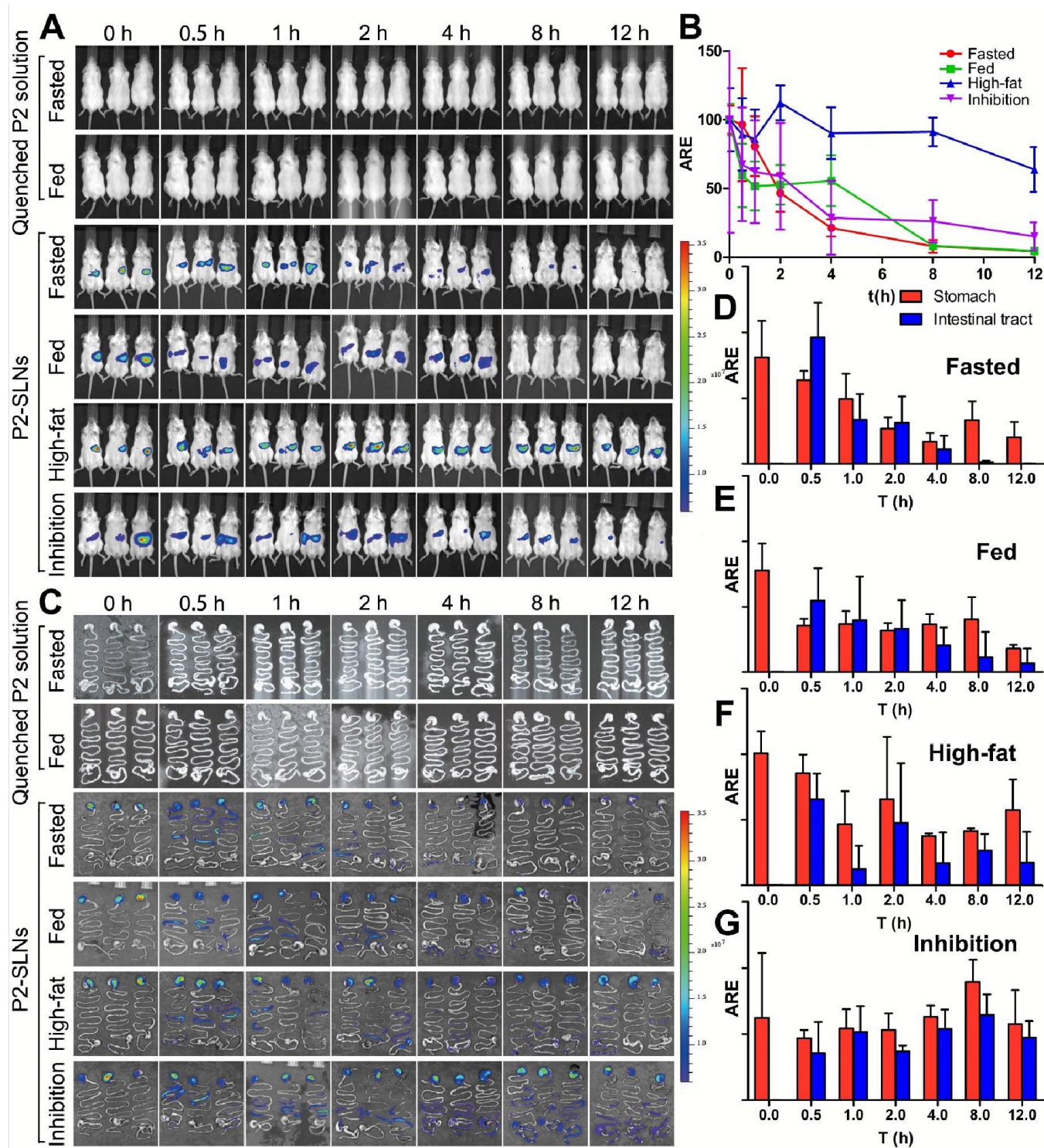


Fig. 1 *In vivo* live imaging pictures of ICR mice after gavage administration of quenched P2 solution and P2-SLN suspension under fasted, fed, high-fat and lipase-inhibition conditions, respectively. A: live imaging; B: quantification based on ARE; C: live imaging of *ex vivo* GI segments; D-G: quantification of various GI segments

delayed gastric emptying rate of SLNs highlights enhanced retention owing to possible reasons of bioadhesion. The extremely low exposure of SLNs in the intestinal tract

suggests fast degradation of SLNs by lipases except in presence of lipase inhibitor. It should also be noted that the disparity in results between *in vivo* and *ex vivo* live imaging

weakens the usefulness of 2D *in vivo* live imaging because of the inability of the latter to accurately locate the position of transit.

Therefore, IVIS spectrum live imaging was coupled with CT to study real-time *in vivo* fate of SLNs. To achieve good imaging, fasted rats were employed in order to exclude the interference of intestinal content. Fig. 2 displays the screenshots of the transit of SLNs in the GI tract at both low and high doses (supplemental videos). Results show that SLNs could be retained in the stomach for prolonged time duration but with decreasing total amount over time. At 1 h, SLNs could be transported to distal ileum regardless of the dose administered. Within 8 h, almost all SLNs were cleared from the GI tract. Scanning the whole body, no fluorescence spots could be observed in any organ or tissue other than the GI tract. The results indicated that there was little chance for translocation of SLNs across the intestinal epithelia; if any, it might be in negligibly small amount.

### Intestinal residence of SLNs and SMMs

The fact that SLNs can transit to the small intestine and reside for a certain time, albeit in limited amount, raises the chance of bioadhesion of SLNs to the intestinal wall. Although *in vivo* live imaging does not find any trace of translocation of SLNs to any organs or tissues other than the GI tract, the possibility of direct interaction of SLNs with GI epithelia should not be excluded. Therefore, we employed an *in situ* perfusion model to study the bioadhesion of SLNs to intestinal mucosae and find evidence whether integral SLNs can be internalized by intestinal epithelia. Fig. 3A shows the fluorescent images of *ex vivo* jejunum segments after *in situ* perfusion. It is obvious that SMMs show stronger fluorescence than SLNs. By measuring ARE, the retention of various formulations is quantified and shown in Fig. 3B. The control group of water-quenched P4 solution shows negligible fluorescence, excluding devotion of fluorescence rekindling to overall fluorescence measurement. In general, SMMs shows significantly higher ARE values than SLNs, and the retention of BS-decorated nanocarriers is a little bit higher than their non-decorated counterparts in each pair. Referring to the compositions and physicochemical properties of both SLNs and SMMs in Table 1, the enhanced retention of SMMs can be possibly ascribed to the relatively small particle size of SMMs and most importantly the mimicking of physiological compositions, which however needs in-depth investigation in the future. After live imaging, the intestine segments were sectioned and observed by fluorescent microscopy to identify traces of fluorescence that might represent internalization of the particles. The P4 channel gives no signal for all four groups, whereas the C6 channel shows sparsely distributed fluorescent signals for SMMs groups

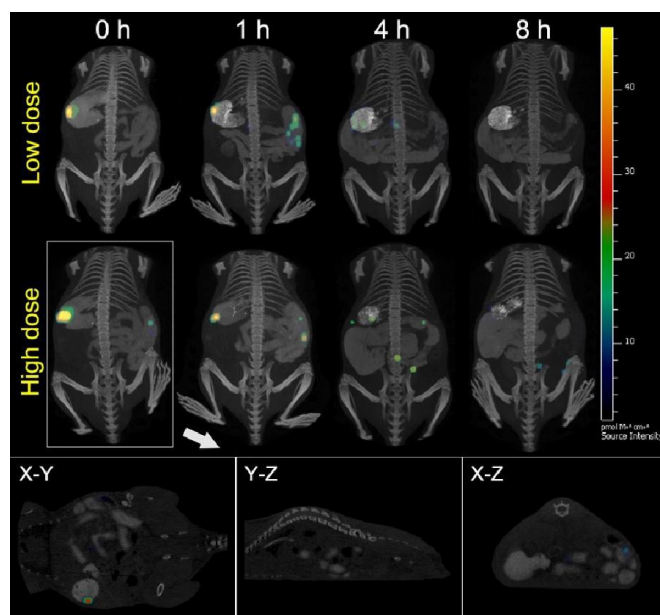


Fig. 2 *In vivo* 3D fluorescence plus CT living imaging of ICR mouse after gavage administration of different dose of P2-SLN in a supine position. The lower part gives the representative X-Y, Y-Z and X-Z position cross-section imaging. Please refer to supplemental videos for panoramic views.

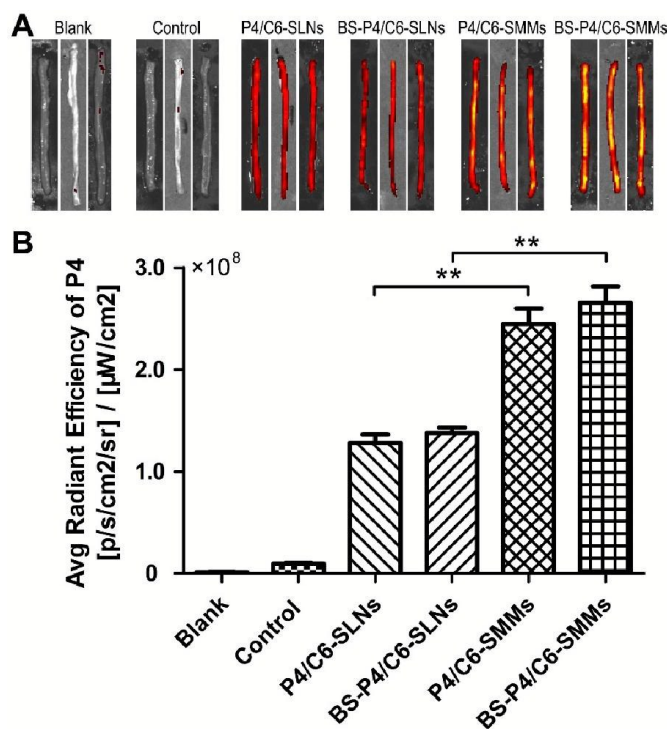


Fig. 3 Live images of *ex vivo* jejunum segments after *in situ* perfusion with different formulations (A); and the corresponding ARE values by measuring P4 fluorescence (B).

that located to the exterior side of the villi, but not to the basal side (Fig. 4). It should be noted that C6 signals may not represent intact particles because free C6 also gives out fluorescence. Theoretically, there should be more fluorescent signals observed since the *ex vivo* bioadhesion study indicates significant retention of the nanocarriers. The lack of fluorescent signals even in the apical side suggests that adhered particles may have been washed out during the fixation, freeze-section and staining process. However, if the particles is internalized integrally into the epithelia, they should not have been washed out completely and fluorescent signals might be observed in the basal side. The disappearance of P4 signals in all test groups serves as strong evidence to confirm there is no absorption of intact particles at all. The absence of non-quenching C6 signals in the basal side further strengthens this conclusion. Even though the C6 signals from SMMs

may associate with the epithelia, intact internalization can be excluded because “micelles” tend to fuse with cell membranes and convey the payload, here C6, into the epithelia.<sup>42</sup>

### Cellular uptake and trans-mono-layer transport

To find more evidence to support our hypothesis that SLNs cannot be internalized as intact particles, we used a series of conventional Caco-2 cell models to study the interaction of SLNs, as well as SMMs for comparison, with cells, especially Caco-2/HT29-MTX cell co-cultures that mimic a mucus layer on the surface of cell monolayers. Several reports by other researchers favoured a mechanism of intact uptake of SLNs through endocytosis.<sup>20,21,25</sup> However, this conclusion is greatly compromised by the fact that their studies were unequivocally carried out on Caco-2 cells

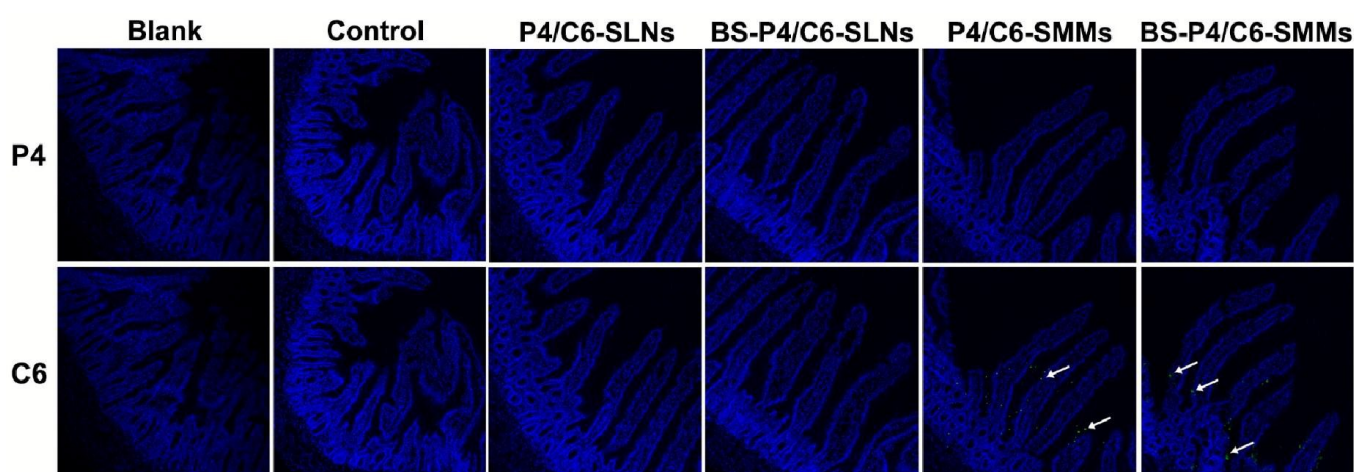


Fig. 4 The CLSM photos of frozen section of rat jejunum after *in situ* perfusion with different formulations either in P4 or C6 channel. The arrows indicate green fluorescent spots found in the C6 channel, but not in the P4 channel in the same tissue specimen.

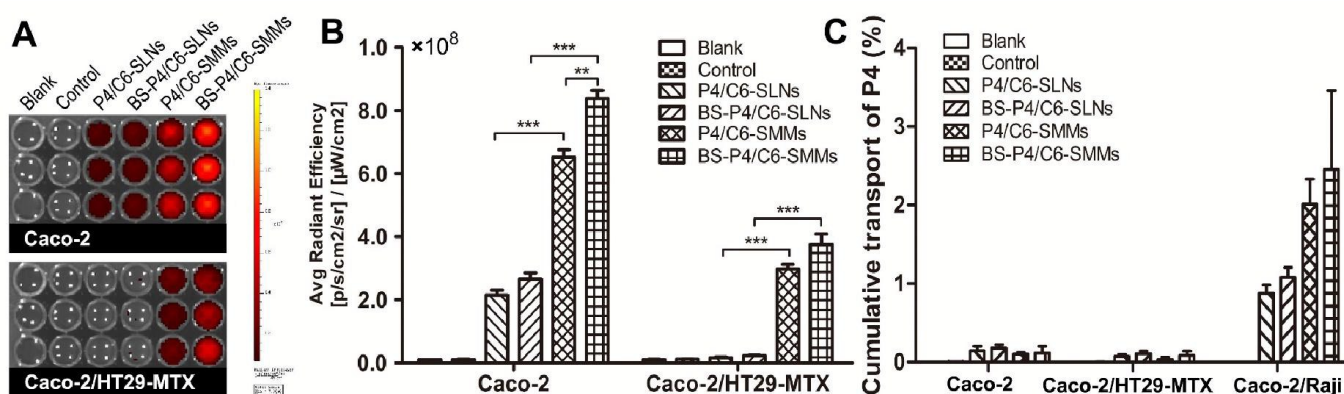


Fig. 5 A: Live images of uptake of different nanocarriers by Caco-2 and Caco-2/HT29-MTX; B: ARE quantitative results of P4 in the well plates; C: cumulative transport of various nanocarriers across different cell monolayers for 2 h by measuring P4 fluorescence.

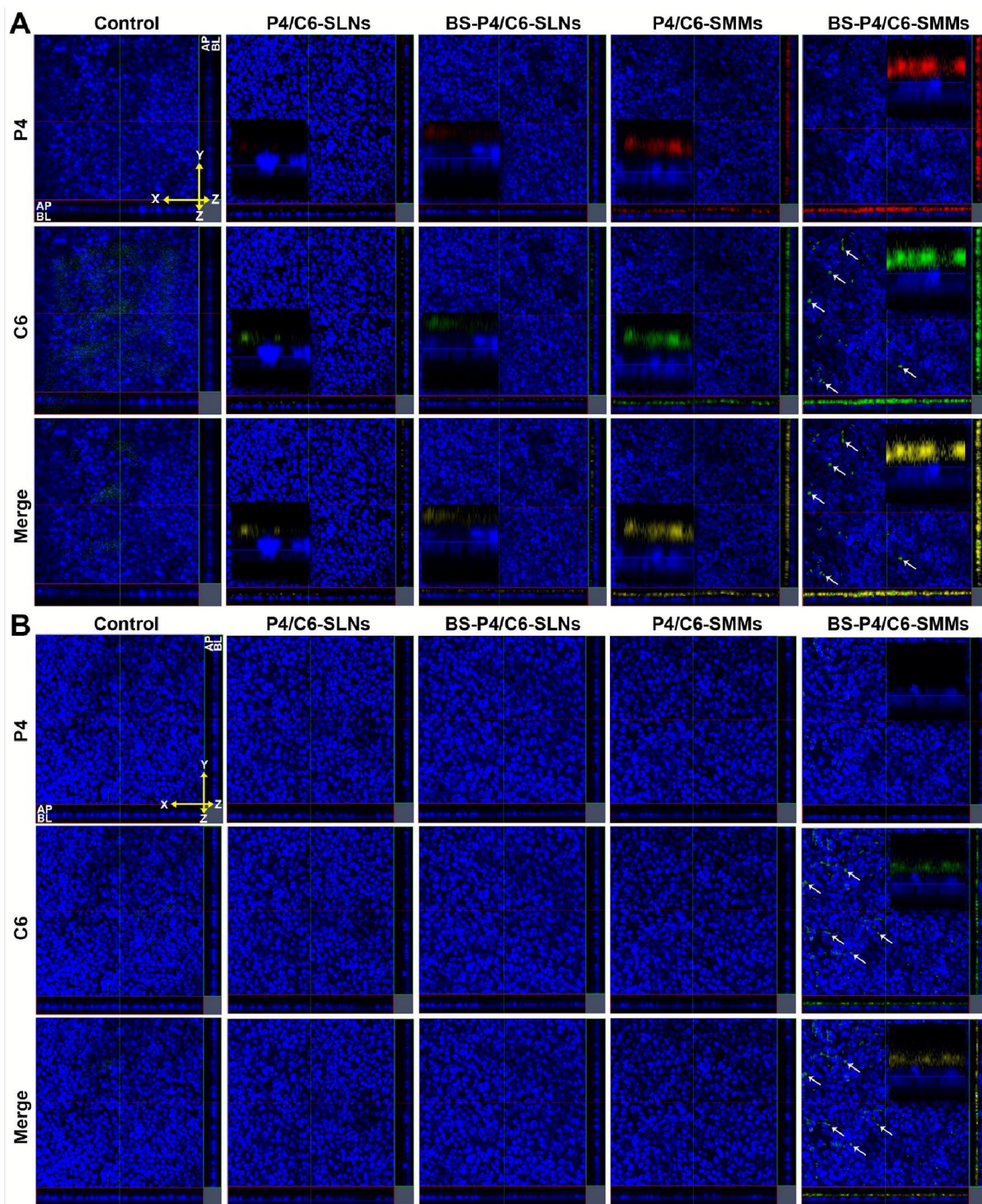


Fig. 6 Confocal microscopic images of Caco-2 (A) and Caco-2/HT29-MTX (B) monolayers incubated with the different SLNs and SMMs. Inlets are enlargement of the X-Z section views of each image that clearly indicate distribution of SLNs-bound fluorescence on the surface of cell monolayers.

and using fluorescent probes that could not identify the particles as a whole. Fig. 5A,B shows the live imaging of cellular uptake of SLNs and SMMs, as well as ARE by measuring P4 fluorescence. The cellular uptake of intact SLNs and SMMs in Caco-2 cell lines is significantly higher than their counterparts in Caco-2/HT29-MTX co-cultures; in each cell model, cellular uptake of SMMs is higher than that of SLNs; in each cell model and either for SLNs or SMMs, BS decoration seems to enhance cellular uptake of the nanocarriers. The results mean that the presence of a mucus layer due to secretion by HT29-MTX cells creates a barrier to the interaction of cells with nanocarriers tested. Whereas the hydrophobicity of SLNs may favour cellular uptake by cell lines, the significantly enhanced uptake by SMMs highlights alternative mechanisms, for instance specific recognition by receptors or transporters, because SMMs simulate physiological compositions. It should also be noted that the cellular uptake of nanocarriers may not necessarily stand for intact internalization because it may be out of bare bioadsorption.

In comparison with cellular uptake, trans-monolayer permeation study is more efficient to identify the transiting behaviour by measuring fluorescence in the receiving chamber in couple with CLSM observation to identify intracellular trafficking. As shown in Fig. 5C, only faint, if not negligible, P4 fluorescence can be measured in the receptor chamber for both Caco-2 and Caco-2/HT29-MTX cell monolayers, indicating that there is no permeation of intact SLNs or SMMs across these two cell monolayers. But P4 signal could be observed in the receiving chamber of Caco-2/Raji cell monolayers, indicating permeation of both SLNs and SMMs. Since Raji cells are generally employed to mimic the function of M cells-associated phagocytosis, the findings above imply that trans-epithelial permeation of intact vehicles, if any, is prone to the M cells pathway. The fact that SMMs show more permeation than SLNs and BS-decoration enhances trans-monolayer permeation raise interesting discussion that physiological compositions in the formulation may enhance adsorption of particles onto cell membranes. In fact, enterocytes are not voracious cells. Although internalization pathways of endocytosis have been observed in Caco-2 cell lines,<sup>20,21,25</sup> they only contribute trivially to the overall absorption of nanocarriers (< 0.2% for Caco-2; < 0.1% for Caco-2/HT29-MTX. Fig. 5C). To the contrary, the M cell pathway is believed to be the principle route of entry of intact particles into the body, but in limited amount subject to limited population of M cells.<sup>43</sup> However, the quantitative contribution of the M cell pathway should be explored and re-evaluated further because the Caco-2/Raji cell models cannot mimic the real situation at the apical side of intestinal epithelia due to lack of a mucus layer. Future studies should employ more sophisticated Caco-2/HT29-

MTX/Raji models with mucus layer at the apical side and phagocytic cell infiltration at the basal side.

By comparing the results of both cellular uptake and trans-monolayer studies, a mechanism of bioadhesion, rather than penetration, is preferred to interpret the interaction of SLNs and SMMs with the cells. CLSM imaging adds strong evidence to support this hypothesis. Fig. 6 show the CLSM images of the monolayers either in P4 or C6 channel. In Caco-2 cell monolayers P4 signals that stands for intact vehicles cannot be found in images of X-Y direction for both SLNs and SMMs, but can be found in X-Z and Y-Z directional images with SMMs show more intense signals. A close enlargement of the images indicates that the fluorescence completely located to the apical side, rightly on the surface of the cells. However, in Caco-2/HT29-MTX cell monolayers, the P4 signals disappear in all directions for SLNs, but are shown faintly for SMMs. The C6 channels show similar signal patterns that can merge well with the P4 channel signals, except that sparsely scattered C6 signals could be found in the X-Y direction images for SMMs. The findings above exclude the possibility of intact uptake of both SLNs and SMMs by cell lines. The most feasible mechanism lies in bioadhesion of nanocarriers to cell surfaces, which is greatly compromised due to the presence of the mucus layer. Since SLNs have more hydrophobic surfaces than SMMs, they encounter more resistance in the mucus layers. Although the hydrophobic domains of the mucus layers may trap SLNs, the overall mucus lining presents a hydrophilic barrier to SLNs. If there is adsorption of SLNs to the apical surface of the monolayers, it must be in a loose state. Originally, we expected more intense accumulation of the nanoparticles in the mucus coating layers, but the results turn out quite the contrary. It can be explained by the fact that both the cellular uptake and trans-monolayer tests involve procedures of washing, e.g. washing with D-Hank's for three times to remove residues of nanocarriers suspension and the reagents used to stain the cells, which may wash out the loosely adhered nanoparticles simultaneously. SMMs can penetrate deep into the mucus layer due to more hydrophilic surfaces and smaller particle size. However, the washing procedures do not affect our judgement on the absence of integral absorption of the nanoparticles because whatever has been taken up by the cell lines cannot be washed out any more and certainly will be detected by CLSM. Instead, payload of SMMs, as represented by C6 signal, can be absorbed into cytoplasm. Furthermore, it should be noted that both *in vitro* and *in vivo* behaviours of the lipid nanocarriers can be affected by their physicochemical properties such as particle size, vehicle structure, surface potential, lipid compositions, surface decoration and so on, which needs to be investigated in future studies.

## Conclusions

The *in vivo* fate of SLNs was monitored using water-quenching NIR fluorescent probe P2 after gastric gavage administration. *In vivo* live imaging in mice indicates very fast degradation of SLNs under both fed and fasted conditions, but significantly delayed degradation under high-fat and lipase-inhibition conditions. Imaging of dissected GI tract segments reveals unexpected findings that a majority of SLNs reside in the stomach, whereas in small intestine SLNs can be degraded quickly. Both high-fat feeding and lipase inhibition lead to significantly slowed gastric emptying rate and prolonged retention of SLNs in the GI tract. No distribution of SLNs in organs or tissues other than the GI tract is observed. *In situ* perfusion results confirm strong adhesion of SLNs as well as SMMs, which simulate the digestive products of SLNs to the intestinal wall. However, cross-section observation using fluorescent microscope eliminate the possibility of permeation of intact vehicles across intestinal epithelia. Cellular uptake of SLNs and SMMs by Caco-2 and Caco-2/HT29-MTX cell lines further confirms bioadhesion of the vehicles to cell membranes. Trans-monolayer permeation study indicates that both vehicles cannot be transported across the monolayers. The presence of a mucus layer due to co-culturing with HT29-MTX cells works as a barrier to the interaction of nanocarriers with cell membranes. SMMs and BS-decoration both enhances bioadhesion and cellular uptake, indicating enhanced bioadhesion due to presence of physiological components. Taking all evidence together, the chances of absorption of intact SLNs via oral delivery seem to be little.

## Acknowledgements

This study was financially supported by Shanghai Commission of Science and Technology (14JC1490300), National Natural Science Foundation of China (81573363, 21372063), and National Key Basic Research Program (2015CB931800).

## Notes and references

- M.A. Iqbal, S. Md, J.K. Sahni, S. Baboota, S. Dang, J. Ali, *J. Drug Target.*, 2012, **20**, 813-830.
- J. Pardeike, A. Hommoss, R.H. Müller, *Int. J. Pharm.*, 2009, **366**, 170-184.
- M. Muchow, P. Maincent, R.H. Muller, *Drug Dev. Ind. Pharm.*, 2008, **34**, 1394-1405.
- Y. Lu, J. Qi, W. Wu, *Curr. Drug Metab.*, 2012, **13**, 396-417.
- E. Kupetz, H. Bunjes, *J. Control. Release*, 2014, **189**, 54-64.
- Y. Funakoshi, Y. Iwao, S. Noguchi, S. Itai, *Int. J. Pharm.*, 2013, **451**, 92-94.
- T. Guo, Y. Zhang, J. Zhao, C. Zhu, N. Feng, *J. Nanobiotechnology*, 2015, **13**, 47.
- A. Patil-Gadhe, A. Kyadarkunte, M. Patole, V. Pokharkar, *Eur. J. Pharm. Biopharm.*, 2014, **88**, 169-177.
- M. Shangguan, J. Qi, Y. Lu, W. Wu, *Int. J. Pharm.*, 2015, **489**, 195-202.
- Y. Liu, G.M. Salituro, K.J. Lee, A. Bak, D.H. Leung, *AAPS PharmSciTech*, 2015, doi:10.1208/s12249-015-0299-8.
- S. Xie, B. Pan, M. Wang, L. Zhu, F. Wang, Z. Dong, X. Wang, W. Zhou, *Nanomedicine (Lond)*, 2010, **5**, 693-701.
- R. Paliwal, S. Rai, B. Vaidya, K. Khatrri, A.K. Goyal, N. Mishra, A. Mehta, S.P. Vyas, *Nanomedicine*, 2009, **5**, 184-191.
- P. Dwivedi, R. Khatik, K. Khandelwal, I. Taneja, K.S. Raju, Wahajuddin, S.K. Paliwal, A.K. Dwivedi, P.R. Mishra, *Int. J. Pharm.*, 2014, **466**, 321-327.
- H. Yuan, C.Y. Chen, G.H. Chai, Y.Z. Du, F.Q. Hu, *Mol. Pharm.*, 2013, **10**, 1865-1873
- X. Zhang, G. Chen, T. Zhang, Z. Ma, B. Wu, *Int. J. Nanomedicine*, 2014, **9**, 5503-5514.
- H. Mu, C.E. Høy, *Prog. Lipid Res.*, 2004, **43**, 105-133.
- C.J. Porter, N.L. Trevaskis, W.N. Charman, *Nat. Rev. Drug Discov.*, 2007, **6**, 231-248.
- H.D. Williams, N.L. Trevaskis, Y.Y. Yeap, M.U. Anby, C.W. Pouton, C.J. Porter, *Pharm. Res.*, 2013, **30**, 2976-2992.
- O.M. Feeney, H.D. Williams, C.W. Pouton, C.J. Porter, *J. Control. Release*, 2014, **192**, 219-227.
- A. Beloqui, M.Á. Solinis, A.R. Gascón, A. del Pozo-Rodríguez, A. des Rieux, V. Prétat, *J. Control. Release*, 2013, **166**, 115-123.
- C. Chen, T. Fan, Y. Jin, Z. Zhou, Y. Yang, X. Zhu, Z.R. Zhang, Q. Zhang, Y. Huang, *Nanomedicine (Lond)*, 2013, **8**, 1085-1100.
- Z. Zhang, F. Gao, H. Bu, J. Xiao, Y. Li, *Nanomedicine*, 2012, **8**, 740-747.
- Z. Yang, M. Chen, M. Yang, J. Chen, W. Fang, P. Xu, *Int. J. Nanomedicine*, 2014, **9**, 327-336.
- N. Zeng, X. Gao, Q. Hu, Q. Song, H. Xia, Z. Liu, G. Gu, M. Jiang, Z. Pang, H. Chen, J. Chen, L. Fang, *Int. J. Nanomedicine*, 2012, **7**, 3703-3718.
- E. Roger, F. Lagarce, E. Garcion, J.P. Benoit, *J. Control. Release*, 2009, **140**, 174-181.
- H. Yuan, J. Chen, Y.Z. Du, F.Q. Hu, S. Zeng, H.L. Zhao, *Colloids Surf. B Biointerfaces*, 2007, **58**, 157-164.
- C. Chen, X. Zhu, Y. Dou, J. Xu, J. Zhang, T. Fan, J. Du, K. Liu, Y. Deng, L. Zhao, Y. Huang, *J. Biomed. Nanotechnol.*, 2015, **11**, 865-876.
- Z. Zhang, H. Bu, Z. Gao, Y. Huang, F. Gao, Y. Li, *Int. J. Pharm.*, 2010, **394**, 147-153.
- X. Hu, J. Zhang, Z. Yu, Y. Xie, H. He, J. Qi, X. Dong, Y. Lu, W. Zhao, W. Wu, *Nanomedicine*, 2015, **11**, 1939-1948.
- W.L. Zhao, E.M. Carreira, *Angew Chem. Int. Ed. Engl.*, 2005, **44**, 1677-1679.
- W.L. Zhao, E.M. Carreira, *Chemistry*, 2006, **12**, 7254-7263.
- H.J. Yao, R.J. Ju, X.X. Wan, Y. Zhang, R.J. Li, Y. Yu, L. Zhang, W.L. Lu, *Biomaterials*, 2011, **32**, 3285-3302.
- R. Silva, H. Carmo, V. Vilas-Boas, D.J. Barbosa, M. Monteiro, P.G. de Pinho, M. de Lourdes Bastos, F. Remião, *Toxicol. Lett.*, 2015, **232**, 271-283.
- M.C. Carey, D.M. Small, *J. Clin. Invest.*, 1978, **61**, 998-1026.
- M.C. Carey, D.M. Small, C.M. Bliss, *Annu. Rev. Physiol.*, 1983, **45**,

- 651-677.
- 36 T. Schersten, *Digestion*, 1973, **9**, 540-553.
- 37 W. Ding, X. Hou, S. Cong, Y. Zhang, M. Chen, J. Lei, Y. Meng, X. Li, G. Li, *Drug Deliv.*, 2015, doi:10.3109/10717544.2015.1020119.
- 38 C. Hilgendorf, H. Spahn-Langguth, C.G. Regårdh, E. Lipka, G.L. Amidon, P. Langguth, *J. Pharm. Sci.*, 2000, **89**, 63-75.
- 39 Martinez-Argudo I, Jepson MA. *Microbiology*, 2008, 154, 3887-3894.
- 40 L. Marciari, R. Faulks, M.S. Wickham, D. Bush, B. Pick, J. Wright, E.F. Cox, A. Fillery-Travis, P.A. Gowland, R.C. Spiller, *Br. J. Nutr.*, 2009, **101**, 919-928.
- 41 K.M. Choi, J. Zhu, G.J. Stoltz, S. Vernino, M. Camilleri, J.H. Szurszewski, S.J. Gibbons, G. Farrugia, *Am. J. Physiol. Gastrointest. Liver Physiol.*, 2007, **293**, G1039-G1045.
- 42 H. Chen, S. Kim, L. Li, S. Wang, K. Park, J.X. Cheng, *Proc. Natl. Acad. Sci. U. S. A.*, 2008, **105**, 6596-6601.
- 43 P. Yeh, H. Ellens, P.L. Smith, *Adv. Drug Deliv. Rev.*, 1998, **34**, 123-133.